Stability analysis of thermally induced spontaneous gas oscillations in straight and looped tubes

Yuki Ueda[a)]
Department of Bio-Applications and Systems Engineering, Tokyo University of Agriculture and Technology, 2-24-16 Nakacho, Koganei, Tokyo 184-8588, Japan

Chisachi Kato
Institute of Industrial Science, The University of Tokyo, 4-6-1 Komaba, Meguroku, Tokyo 153-8505, Japan

(Received 5 December 2007; revised 8 May 2008; accepted 9 May 2008)

A gas in a tube spontaneously oscillates when the temperature gradient applied along the wall of the tube is higher than the critical value. This spontaneous gas oscillation is caused by the thermal interaction between the gas and the tube wall. The stability limit of the thermally induced gas oscillation is numerically investigated by using the linear stability theory and a transfer matrix method. It is well known that an acoustic wave excited by the spontaneous gas oscillation occurring in a looped tube is different from that in a straight tube with two ends; a traveling acoustic wave is induced in a looped tube, whereas a standing acoustic wave is caused in a straight tube. The conditions for the stability limits in both tube types were calculated. The calculated and measured conditions were compared and were found to be in good agreement. Calculations performed by varying the value of the Prandtl number of the gas were used to determine the reasons for the existence of the stability limits of the looped and straight tubes.
 [DOI: 10.1121/1.2939134]

PACS number(s): 43.35.Ud [RR] Pages: 851–858

I. INTRODUCTION

When the temperature gradient imposed along the wall of a tube exceeds a critical value, the gas in the tube begins to oscillate, so that an acoustic wave is excited. This spontaneous gas oscillation is sustained by the energy conversion from heat to acoustic power occurring through the thermal contacts between the gas and the wall of the tube.

The spontaneous gas oscillation can be classified into two types based on the characteristics of the thermally induced acoustic wave. One type of gas oscillation occurs in a tube with two ends, i.e., a straight tube, which excites a standing acoustic wave. The other type of gas oscillation occurs in a looped tube, which causes a traveling acoustic wave.

Rott[1,2] and Rott and Zouzoulas[3] analytically investigated the stability limit of gas oscillation in a straight tube by employing a strict linearization of all basic equations, and they derived the stability curves for the temperature ratio against the tube radius relative to the thickness of the viscous boundary layer. Yazaki *et al.* compared their experimentally obtained stability curves with Rott's analytical ones; this comparison revealed a good agreement between the experimentally and analytically obtained curves.[4] A number of studies have investigated the stability curves in a straight tube.[5–9] This provides a basic understanding of the spontaneous gas oscillation in a straight tube.

The spontaneous gas oscillation in a looped tube has recently attracted more attention compared with that in a tube with two ends; thus, most of the recent work in thermoacoustics has dealt with spontaneous gas oscillation in a looped tube rather than that in a straight tube.[10–12] This is because a traveling acoustic wave can realize an efficient energy conversion.[13,14] Yazaki *et al.* measured the conditions for the stability limit of the spontaneous gas oscillation in a looped tube, and they studied the stability curve of the looped tube.[15] Tanaka[16] and Penelet *et al.*[17] succeeded in calculating the conditions for the stability limit. However, in the case of the looped tube, very few studies have numerically investigated the conditions for the stability limit in detail.

In this paper, we calculate the conditions for the stability limit of the thermally induced gas oscillation in both looped and straight tubes by using the linear stability theory and a transfer matrix method. It will be shown that the obtained calculation results qualitatively agree with the experimental results. By using the calculation in which the Prandtl number of a gas is varied, we address the reasons for the existence of the stability limit in looped and straight tubes.

In Sec. II, the numerically investigated looped and straight tubes are mentioned; in Sec. III, the method for calculating the stability limit of the thermally induced spontaneous gas oscillation is described. Section IV provides the calculation results of the stability curve and compares these results with the experimental results. The calculation results are analyzed in detail in Sec. V. The summary of the results is provided in Sec. VI.

II. CALCULATION MODEL

A. Looped tube and straight tube

The numerically investigated tubes are schematically illustrated in Fig. 1. The total length of the looped and straight

[a)]Electronic mail: uedayuki@cc.tuat.ac.jp

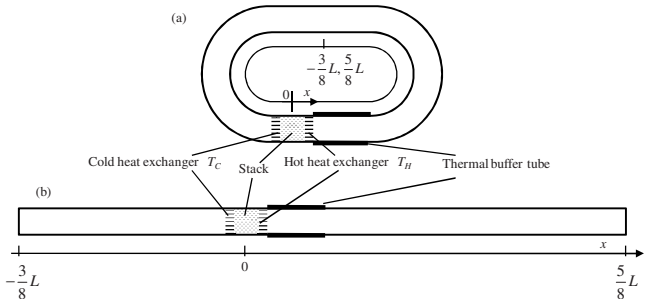

FIG. 1. Schematic illustrations of (a) a looped tube and (b) a straight tube.

tubes is denoted as L. Both tubes are filled with atmospheric air and can be divided into six components: waveguide 1, cold heat exchanger, *stack*, hot heat exchanger, thermal buffer tube, and waveguide 2. The radius of the waveguides and thermal buffer tube is denoted as r_{tube}, and the length of the thermal buffer tube is denoted as L_{tb}. The stack is composed of a porous material with several narrow circular channels. The inner radius of the narrow circular channels in the stack is denoted as r_{stack}. The length of the stack is L_{stack}. The stack is placed between cold and hot heat exchangers; these exchangers are composed of flat plates set in parallel with a spacing of $2r_{\text{hx}}$. The length of the plates is L_{hx}. The porosity of the stack is ϵ_{stack}, and that of the heat exchangers is ϵ_{hx}. In this study, porosity is defined as the ratio of the total cross-sectional area of the flow channels in the stack/heat exchanger to the area of the tube (πr_{tube}^2).

The coordinate x is defined along the axis of the tube. This coordinate is used for both looped and straight tubes. The origin of x is set at the center of the stack. In the case of the straight tube, the closed ends are located at $x=-3L/8$ and at $x=5L/8$ so that the center of the stack will be set at the midpoint of a pressure node and a velocity node of a nonviscous standing wave with a wavelength $\lambda=L$. Due to this condition, the frequency of the gas oscillation occurring in the straight tube is the same as that occurring in the looped tube. In the case of the looped tube, $x=-3L/8$ and $x=5L/8$ represent the same position.

B. Temperature distribution along the axes of the tubes

The calculation method proposed below requires the temperature distribution to be along the tube axis. The mean temperature T_m of the gas in both tubes is assumed to be distributed, as shown in Fig. 2. T_m is maintained at a constant value except from $x=-X_1$ to X_1 (in the stack) and from $x=X_2$ to X_3 (in the thermal buffer tube), where $X_1=L_{\text{stack}}/2$, $X_2=X_1+L_{\text{hx}}$, and $X_3=X_2+L_{\text{tb}}$.

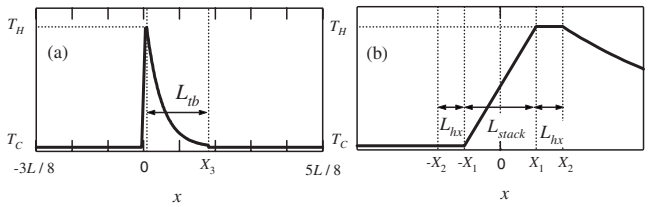

FIG. 2. Temperature distribution (a) along the tube and (b) near the stack.

In the stack (from $x=-X_1$ to X_1), T_m increases linearly from T_C to T_H [see Fig. 2(b)]. The reason for the assumption of linear temperature distribution in the stack is as follows: the stacks used in the experiments performed by several researchers are essentially insulated. Therefore, the temperature distribution in the absence of spontaneous gas oscillation would become linear due to thermal conduction along the axial direction.

In the thermal buffer tube (from $x=X_2$ to X_3), T_m decreases exponentially,

$$T_{m,\text{tb}}(x) = (T_H - T_C)\exp\left(-\frac{x-X_2}{R}\right) + T_C. \tag{1}$$

The coefficient in this equation, R, was varied in the calculation. At $x=X_3$, T_m discontinuously changes, as can be seen in Fig. 2(a). This is because $T_{m,\text{tb}}(X_3)-T_C=(T_H-T_C)\exp(-L_{\text{tb}}/R)>0$. We numerically confirmed that when $L_{\text{tb}}/R>4$, the temperature difference $T_{m,\text{tb}}(X_3)-T_C$ has a negligible influence on the calculated stability limit of the present tubes.

III. CALCULATION METHOD

This section describes the method for calculating the stability limit of the thermally driven spontaneous gas oscillation in the tubes. This calculation is based on Rott's thermoacoustic theory[1] and the transfer matrix method for oscillatory pressure P and volume velocity U. The time variation of the pressure and volume velocity is given by the factor $\exp(i\omega t)$. Generally, ω is represented as a complex quantity; its real and imaginary parts represent the angular frequency of the gas oscillation and the logarithmic amplification, respectively. At the stability limit, the logarithmic amplification becomes zero. Therefore, ω has only a real part.

A. Transfer matrix

In this subsection, the calculation method of the transfer matrix of the components (which are the waveguides, heat exchangers, stack, and thermal buffer tube) is described. Using Rott's acoustic approximation,[1] the momentum and continuity equations in a flow channel are written[18] as

$$\frac{dP}{dx} = -\frac{1}{A}\frac{i\omega\rho_m}{1-\chi_\nu}U, \tag{2}$$

$$\frac{dU}{dx} = -\frac{i\omega A[1+(\gamma-1)\chi_\alpha]}{\gamma P_m}P + \frac{\chi_\alpha-\chi_\nu}{(1-\chi_\nu)(1-\sigma)}\frac{1}{T_m}\frac{dT_m}{dx}U, \tag{3}$$

respectively, where A is the cross-sectional area of the channel, and ρ_m, P_m, γ, and σ are the mean density, the mean pressure, the ratio of specific heats, and the Prandtl number of the working gas, respectively. Here, the assumption that the heat capacity of the channel wall is considerably larger than that of the working gas is used. χ_α and χ_ν are complex functions that allow us to describe the three-dimensional phenomena in the channel using the two one-dimensional equations. For example, in a circular channel with radius r,

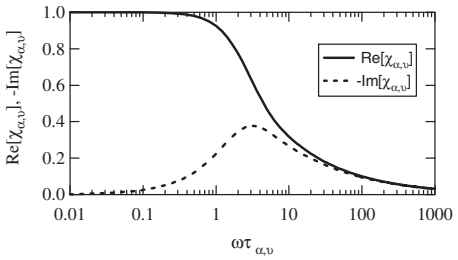

FIG. 3. Complex functions χ_α and χ_ν.

$$\chi_\alpha = \frac{2J_1(Y_\alpha)}{Y_\alpha J_0(Y_\alpha)}, \tag{4}$$

$$\chi_\nu = \frac{2J_1(Y_\nu)}{Y_\nu J_0(Y_\nu)},$$

$$Y_\alpha = (i-1)\sqrt{\omega\tau_\alpha}, \quad Y_\nu = (i-1)\sqrt{\omega\tau_\nu}, \tag{5}$$

where J_1 and J_0 are the first- and zeroth-order Bessel functions, respectively, and τ_α and τ_ν are the thermal and viscous relaxation times, respectively. τ_α is defined as $\tau_\alpha = r^2/(2\alpha)$ and τ_ν as $\tau_\nu = r^2/(2\nu)$, where α and ν are the thermal diffusivity and kinematic viscosity, respectively. $\omega\tau_\alpha$ and $\omega\tau_\nu$ can also be described by r and the thicknesses of the thermal boundary layer, δ_α, and of the viscous boundary layer, δ_ν, as $\omega\tau_\alpha = (r/\delta_\alpha)^2$ and $\omega\tau_\nu = (r/\delta_\nu)^2$, respectively. $\omega\tau_\alpha$ and $\omega\tau_\nu$ are related by $\sigma = \nu/\alpha$ as $\omega\tau_\alpha/\sigma = \omega\tau_\nu$. Figure 3 shows χ_α and χ_ν of the circular channel as a function of $\omega\tau_\alpha$ and $\omega\tau_\nu$, respectively.

Equations (2) and (3) can be modified in a matrix form as follows:

$$\frac{d}{dx}\begin{pmatrix} P(x,t) \\ U(x,t) \end{pmatrix} = C(x)\begin{pmatrix} P(x,t) \\ U(x,t) \end{pmatrix},$$

$$C(x) \equiv \begin{pmatrix} 0 & -\frac{1}{A}\frac{i\omega\rho_m}{1-\chi_\nu} \\ -\frac{i\omega A[1+(\gamma-1)\chi_\alpha]}{\gamma P_m} & \frac{\chi_\alpha - \chi_\nu}{(1-\chi_\nu)(1-N_{\mathrm{Pr}})}\frac{1}{T_m}\frac{dT_m}{dx} \end{pmatrix}. \tag{6}$$

Here, it should be noted that ρ_m, γ, χ_ν, χ_α, and σ depend on T_m, i.e., on x.

When the (2,2) element of C (c_{22}) becomes zero, the matrix C represents the well-known wave equation of a plane sound wave propagating in a channel.[19] Hence, c_{22}, which is the second term on the right-hand side of Eq. (3), plays an important role in the stability of spontaneous gas oscillation.

1. Without temperature gradient

When $dT_m/dx = 0$. Eq. (6) can be solved analytically. This is because γ, χ_ν, χ_α, and σ are independent of x, and the second term on the right-hand side of Eq. (3) vanishes. When the pressure and volume velocity at point x_0 are denoted by P_0 and U_0, respectively, the solution can be expressed as

$$\begin{pmatrix} P(x,t) \\ U(x,t) \end{pmatrix} = M_{\mathrm{I}}(x,x_0)\begin{pmatrix} P_0(x_0,t) \\ U_0(x_0,t) \end{pmatrix},$$

$$M_{\mathrm{I}}(x,x_0) \equiv \begin{pmatrix} \cos[k(x-x_0)] & \frac{-i\omega\rho_m \sin[k(x-x_0)]}{Ak(1-\chi_\nu)} \\ \frac{Ak(1-\chi_\nu)\sin[k(x-x_0)]}{i\omega\rho_m} & \cos[k(x-x_0)] \end{pmatrix}. \tag{7}$$

Here, k is the complex wave number given by

$$k = \frac{\omega}{a}\sqrt{\frac{1+(\gamma-1)\chi_\alpha}{1-\chi_\nu}}, \tag{8}$$

where a is the adiabatic sound speed. Equation (7) shows that when P and U are specified for one point, the distributions of P and U along the tube without the temperature gradient can be calculated.

2. With temperature gradient

When $dT_m/dx \neq 0$, it is difficult to solve Eq. (6) analytically. Hence, it is computationally integrated. By applying a forward difference scheme using the fourth-order Runge–Kutta method to Eq. (6),

$$\begin{pmatrix} P(x+\Delta x,t) \\ U(x+\Delta x,t) \end{pmatrix} = (E + \Delta x C'(x))\begin{pmatrix} P(x,t) \\ U(x,t) \end{pmatrix},$$

$$C'(x) = \tfrac{1}{6}(\mathrm{RK}_A + 2\mathrm{RK}_B + 2\mathrm{RK}_C + \mathrm{RK}_D),$$

$$\mathrm{RK}_A = C(x),$$

$$\mathrm{RK}_B = C(x+\Delta x/2)\left(E + \frac{\Delta x}{2}\mathrm{RK}_A\right),$$

$$\mathrm{RK}_C = C(x+\Delta x/2)\left(E + \frac{\Delta x}{2}\mathrm{RK}_B\right),$$

$$\mathrm{RK}_D = C(x+\Delta x)(E + \Delta x \mathrm{RK}_C) \tag{9}$$

can be obtained, where E is a unit matrix. Hence,

$$\begin{pmatrix} P(x,t) \\ U(x,t) \end{pmatrix} = M_{\mathrm{II}}(x,x_0)\begin{pmatrix} P_0(x_0,t) \\ U_0(x_0,t) \end{pmatrix},$$

$$M_{\mathrm{II}}(x,x_0) \equiv (E + \Delta x C'_{n-1})(E + \Delta x C'_{n-2}) \cdots (E + \Delta x C'_1)(E + \Delta x C'_0) \tag{10}$$

is obtained. Here, n is the number of partitions between x_0 and x, Δx is defined as $(x-x_0)/n$, and C'_j represents C' at $x = x_0 + j\Delta x$. This equation shows that despite the temperature gradient being imposed along the thermal buffer tube/stack, when P and U are provided at one position, the distributions of P and U can be calculated.

B. Method for calculating stability limit

Since T_m is maintained at the constant value from $x=-3L/8$ to $-X_2$, [see Figs. 2(a) and 2(b)], the transfer matrix $M_{\mathrm{I},1}$ of this region was calculated by using M_{I}. Similarly, the transfer matrices for $x=-X_2$ to $-X_1$ (the cold heat exchanger), for $x=X_1$ to X_2 (the hot heat exchanger), and for $x=X_3$ to $5L/8$ are calculated and are denoted by $M_{\mathrm{I,chx}}$, M_{Ihhx}, and $M_{\mathrm{I},2}$, respectively.

Equation (10) was used to compute the transfer matrices $M_{\mathrm{II},s}$ for $x=-X_1$ to X_1 (the stack) and $M_{\mathrm{II,tb}}$ for $x=X_2$ to X_3 (the thermal buffer tube). The partition number $n=100$ was used because it was confirmed that the calculated stability limits with $n=100$, 200, and 400 are almost similar.

Using $M_{\mathrm{I},1}$, $M_{\mathrm{I,chx}}$, $M_{\mathrm{I,hhx}}$, $M_{\mathrm{I},2}$, $M_{\mathrm{II},s}$, and $M_{\mathrm{II},l}$, the transfer matrix of the looped and straight tubes, M_{all}, is written as

$$M_{\mathrm{all}} = M_{\mathrm{I},2} M_{\mathrm{II},l} M_{\mathrm{I,hhx}} M_{\mathrm{II},s} M_{\mathrm{I,chx}} M_{\mathrm{I},1}. \tag{11}$$

Note that in the present study, we did not take account of nonlinear effects, such as the "minor loss,"[20] occurring at the connecting point between the components. By using M_{all}, the oscillatory pressure P_a and volume velocity U_a at $x=-3L/8$ are related to the oscillatory pressure P_b and volume velocity U_b at $x=5L/8$ as

$$M_{\mathrm{all}} \begin{pmatrix} P_a \\ U_a \end{pmatrix} = \begin{pmatrix} P_b \\ U_b \end{pmatrix}. \tag{12}$$

By using this equation, we calculated the stability limit of the thermally induced gas oscillation.

1. For the looped tube

Since $x=-3L/8$ and $x=5L/8$ represent the same position in the looped tube, Eq. (12) can be rewritten as

$$M_{\mathrm{all}} \begin{pmatrix} P_a \\ U_a \end{pmatrix} = \begin{pmatrix} P_a \\ U_a \end{pmatrix}. \tag{13}$$

The solution (P_a, U_a) of Eq. (13) is nonzero if the determinant of the matrix $(M_{\mathrm{all}}-E)$ is zero, i.e., if

$$(m_{11}-1)(m_{22}-1) - m_{12}m_{21} = 0, \tag{14}$$

where E is the unit matrix and m_{ij} is the element of M_{all}. Therefore, by solving Eq. (14), we can achieve the condition of the stability limit of the spontaneous gas oscillation induced in the looped tube.

2. For the straight tube

For the straight tube, Eq. (12) can be modified as

$$M_{\mathrm{all}} \begin{pmatrix} P_a \\ 0 \end{pmatrix} = \begin{pmatrix} P_b \\ 0 \end{pmatrix}. \tag{15}$$

This is because the volume velocity at $x=-3L/8$ and $x=5L/8$ must be zero due to the closed ends. P_a and P_b in Eq. (15) are nonzero if m_{21} is zero, i.e., if

$$m_{21} = 0. \tag{16}$$

Therefore, Eq. (16) determines the condition of the stability limit in the straight tube.

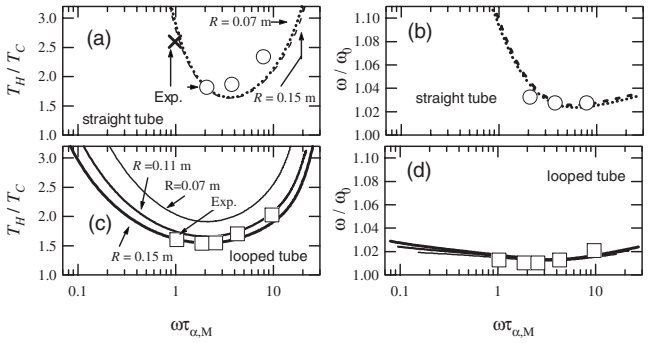

FIG. 4. The conditions of the stability limit of [(a) and (b)] the straight tube and [(c) and (d)] the looped tube. The temperature ratio T_H/T_C and frequency ratio ω/ω_0 of the stability limit are plotted as a function of $\omega\tau_{\alpha,M}$.

IV. CALCULATION RESULTS

A. Calculation condition

In the calculation described below, we chose r_{stack} and T_H as the variable parameters and defined $L=2.8$ m, $L_{\mathrm{stack}}=35$ mm, $L_{\mathrm{hx}}=13$ mm, $L_{\mathrm{tb}}=0.60$ m, $r_{\mathrm{tube}}=20$ mm, $r_{\mathrm{hx}}=0.5$ mm, $\epsilon_{\mathrm{hx}}=0.67$, and $T_C=295$ K. These values are the same as those in the experiment described later in Sec. IV B. Although the porosity $\epsilon_{\mathrm{stack}}$ of the stacks used for the experiment were between 0.69 and 0.87, $\epsilon_{\mathrm{stack}}$ in the calculation was assumed to be the same as ϵ_{hx}, i.e., $\epsilon_{\mathrm{stack}}=0.67$. The coefficient R in Eq. (1) was varied from 0.07 to 0.15 m. The reason why the values of R were selected to be in this range is as follows. We experimentally measured the temperature distribution along the thermal buffer tube: when the gas oscillation did not take place, the measured R was 0.07 m; on the other hand, when the gas oscillation occurred, R in the case of the looped tube had values between 0.07 and 0.15 m, whereas R for the straight tube was approximately 0.07 m.

In order to calculate the values of ν, α, ρ_m, γ, and c_p, we used polyfunctions fitting their temperature dependences.[21] The number of polynomial terms of the polyfunctions was 6.

B. Stability limit

The left-hand sides of Eqs. (14) and (16) were computed as a function of real ω with various T_H and r_{stack}; further, the combinations of ω/ω_0, T_H/T_C, and $\omega\tau_{\alpha,M}$ satisfying Eqs. (14) and (16) were determined. ω/ω_0, T_H/T_C, and $\omega\tau_{\alpha,M}$ are dimensionless parameters corresponding to ω, T_H, and r_{stack}, respectively. Here, ω_0 is defined as $\omega_0=2\pi a_0/L$, where $a_0=340$ m/s, and $\omega\tau_{\alpha,M}$ is defined using thermal diffusivity at the center of the stack $x=0$, where the temperature $T_M=(T_H+T_C)/2$. Although the combinations thus obtained revealed that spontaneous gas oscillation occurs in several frequency modes, we focus on the calculation results of a mode at $\omega/\omega_0 \sim 1$.

In Fig. 4, the calculated conditions of the stability limit are denoted by lines; the calculated T_H/T_C and ω/ω_0 are shown as a function of $\omega\tau_{\alpha,M}$. First, we see the calculated T_H/T_C of the straight tube. The calculated results for the straight tube with $R=0.07$ m and that with $R=0.15$ m are shown in Fig. 4(a) by dotted and dashed lines, respectively. However, it is difficult to distinguish the dashed line from the dotted line. This indicates that T_H/T_C of the straight tube is

almost independent of the value of R. The value of T_H/T_C takes a minimum value at $\omega\tau_{\alpha,M}\sim 3$, and the T_H/T_C curve is U shaped. Figure 4(b) shows that ω/ω_0 is also independent of the value of R and increases rapidly with a decrease in $\omega\tau_{\alpha,M}$ from $\omega\tau_{\alpha,M}\sim 3$. These results are identical to the characteristics of the curves obtained by Rott and Zouzoulas[3] and Yazaki *et al.*[4]

Next, we focus on the calculation results of the looped tube, which are shown in Figs. 4(c) and 4(d). Figure 4(c) shows that the value of T_H/T_C of the looped tube depends on the value of R. However, it was found that independent of the value of R, T_H/T_C at a given R takes a minimum value near $\omega\tau_{\alpha,M}=2$. Moreover, it was shown that the shapes of the three T_H/T_C curves of the looped tube are very similar.

The calculated $\omega\tau_{\alpha,M}$ dependences of T_H/T_C of the looped tube are similar to those of the straight tube for $\omega\tau_{\alpha,M}>3$. However, as can be seen from Figs. 4(a) and 4(c), for $\omega\tau_{\alpha,M}<3$, the $\omega\tau_{\alpha,M}$ dependences of T_H/T_C of the looped tube are different from those of the straight tube; as $\omega\tau_{\alpha,M}$ decreases, T_H/T_C of the looped tube increases gradually compared with that of the straight tube. As a result, when $\omega\tau_{\alpha}\ll 3$, T_H/T_C at the stability limit of the looped tube would be considerably lower than that of the straight tube, regardless of the value of R. Figures 4(b) and 4(d) show that the curves of ω/ω_0 of the looped tube also differ from those of the straight tube for $\omega\tau_{\alpha,M}<3$.

C. Comparison of calculation with experiment

In order to compare the calculated and experimental values of T_H/T_C and ω/ω_0, we performed the measurements of T_H/T_C and ω/ω_0. We constructed the looped and straight tubes shown in Figs. 1(a) and 1(b). The looped tube consisted of stainless-steel tubes and four 90° elbows, whereas the straight tube consisted of stainless-steel tubes. Ceramic honeycombs comprising square channels were used as stacks in the experiments, whereas the stacks used in the calculations were assumed to have circular channels. Half of the hydraulic diameter[22] of the stacks was used as r_{stack} for the experiments. We considered that the difference in the geometry of the channels in the experiments and calculations had a negligible effect on the stability limit because the relation between $\chi_{\alpha,\nu}$ and $\omega\tau_{\alpha,\nu}$ of a square channel is very similar to that of a circular channel.[18,23] The hot and cold heat exchangers used in the experiments comprised flat brass plates set in parallel with a spacing. The thickness of the flat brass plates was 0.5 mm. The dimensions of the constructed tubes (the total tube length L, the stack length L_{stack}, the length of the heat exchangers, L_{hx}, the radius of the tubes, r_{tube}, and the spacing in the heat exchangers, $2r_{\mathrm{hx}}$,) were the same as those in the calculation.

The hot heat exchanger was heated by an electric heater wound around it. The cold heat exchanger was cooled with chilled water (≈295 K) passing through the tube wound around it. It was experimentally confirmed that the temperature difference across the cross section of the hot heat exchanger was up to 20 K, whereas the temperature difference across the cross section of the cold heat exchanger was up to 5 K. We defined the averaged temperatures across the cross section of the hot and cold heat exchangers as T_H and T_C, respectively.

We measured the pressure by using a pressure sensor mounted on the tube wall near the stack with increasing T_H and determined the condition of the stability limit experimentally. In Figs. 4(a) and 4(c), the measured T_H/T_C at the stability limit in the straight tube and that in the looped tube are plotted with open circles and open squares, respectively. When stacks with $r_{\mathrm{stack}}=0.30$ and 0.40 mm were used, spontaneous gas oscillation was not observed in the straight tube for $T_H/T_C<2.6$, which is the experimental upper limit of T_H/T_C. When $T_H/T_C=2.6$ and $\omega/\omega_0=1.05\pm 0.05$ are assumed, $\omega\tau_{\alpha,M}$ of the stack with $r_{\mathrm{stack}}=0.40$ mm is evaluated to be 1.04 ± 0.05. These results prove that the gas in the straight tube is stable in the region ($\omega\tau_{\alpha,M}<1.04$, $T_H/T_C<2.6$). In order to show this result, we plotted the multiplication sign × at $(\omega\tau_{\alpha,M},T_H/T_C)=(1.04,2.6)$ in Fig. 4(a).

As observed in Fig. 4(a), the experimentally obtained T_H/T_C of the straight tube quantitatively agrees with the calculated T_H/T_C. Figure 4(c) shows that the measured T_H/T_C of the looped tube takes the minimum value at $\omega\tau_{\alpha,M}\sim 2$ and gradually increases compared with that of the straight tube below $\omega\tau_{\alpha,M}=2$. This result is the same as the calculated results. Therefore, we consider that the measured T_H/T_C of the looped tube is also in qualitative agreement with the calculated T_H/T_C.

The symbol in Figs. 4(b) and 4(d) show the measured ω/ω_0 at the stability limits. These figures also show that for both tube types, the measured ω/ω_0's agree well with the calculated ratios. Based on the agreement of T_H/T_C and ω/ω_0, we conclude that the proposed calculation method succeeds in modeling the stability limit of the thermally induced spontaneous gas oscillation in looped and straight tubes.

V. ANALYSIS OF THE STABILITY LIMIT

A. Temperature ratio T_H/T_C at the stability limit

As mentioned above, the calculated T_H/T_C's of both looped and straight tubes take minimum values, and the T_H/T_C curves are U shaped. In this subsection, the reasons for the existence of the stability limit are determined.

The $\omega\tau_{\alpha,M}$ dependency of T_H/T_C for $\omega\tau_{\alpha,M}>3$ can be understood from the $\omega\tau_{\alpha,\nu}$ dependency of $\chi_{\alpha,\nu}$. As shown in Fig. 3, $\mathrm{Re}[\chi_{\alpha,\nu}]$ and $\mathrm{Im}[\chi_{\alpha,\nu}]$ approach zero for $\omega\tau_{\alpha,\nu}\gg 3$. This reduces the value of the second term on the right-hand side of Eq. (3); when $\chi_{\alpha,\nu}$ is zero, the second term is also zero. Since the second term is the origin of the driving force for spontaneous gas oscillation, T_H/T_C required for the excitation of the oscillation increases when $\omega\tau_{\alpha,M}$ increases from 3.

Understanding the $\omega\tau_{\alpha,M}$ dependency of T_H/T_C for $\omega\tau_{\alpha,M}<3$ is more difficult than understanding that for $\omega\tau_{\alpha,M}>3$. This is because P and U are complex and when $\omega\tau_{\alpha,\nu}$ decreases below 3, $\mathrm{Re}[\chi_{\alpha,\nu}]$ increases whereas $\mathrm{Im}[\chi_{\alpha,\nu}]$ decreases. In order to understand the $\omega\tau_{\alpha,M}$ dependency of T_H/T_C for $\omega\tau_{\alpha,M}<3$, we consider the physical meaning of $\omega\tau_{\alpha,\nu}$. A decrease in $\omega\tau_{\nu}$ simply increases the

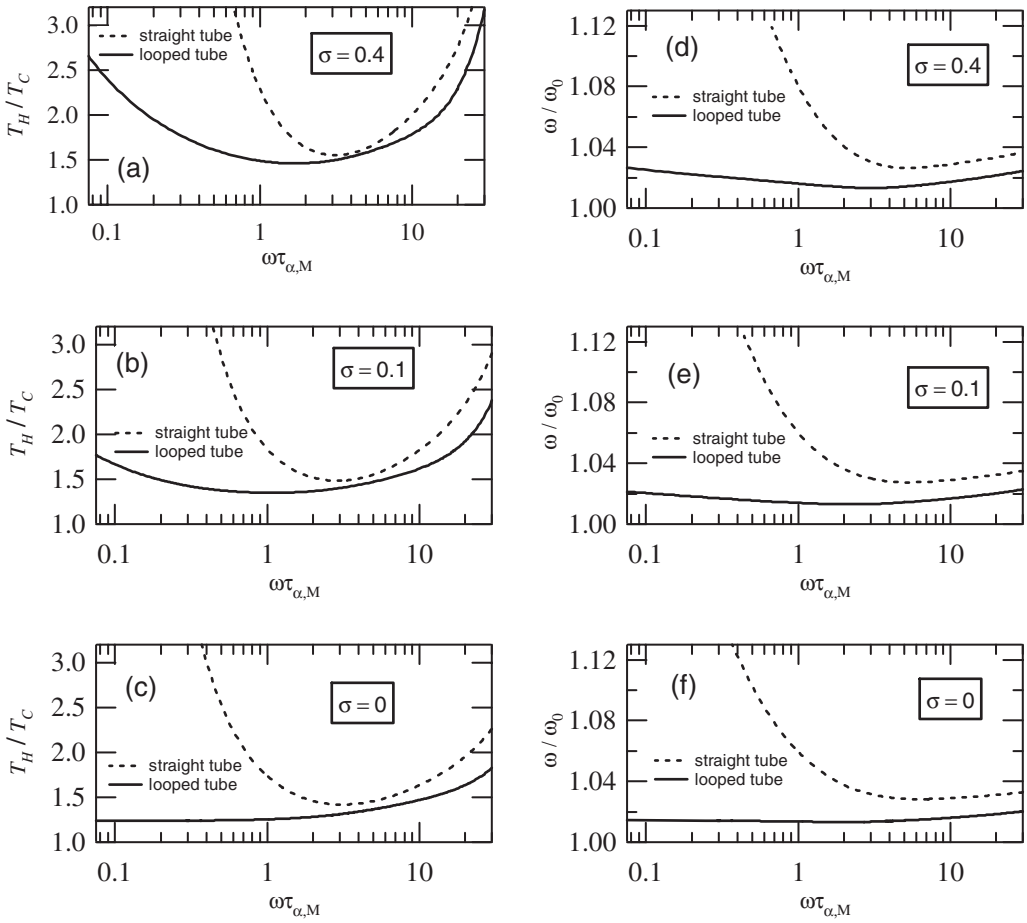

FIG. 5. Stability curves in the looped tube (solid line) and straight tube (dashed line). The stability curves are calculated with a variety of the value of the Prandtl number σ in the stack.

effect of the viscosity. On the other hand, a decrease in $\omega\tau_\alpha$ modifies the thermal process of heat exchange between the gas and channel wall due to the effect of the thermal conductivity of the gas. When $\omega\tau_\alpha \ll 3$, the thermal relaxation time τ_α is much shorter than the cyclic period $2\pi/\omega$; therefore, heat exchange occurs instantaneously, i.e., isothermally (reversibly). When $\omega\tau_\alpha \sim 3$, heat exchange occurs irreversibly because $\tau_\alpha \sim 2\pi/\omega$. Based on the discussion regarding entropy oscillation along the radial direction of a flow channel, Tominaga stated that irreversibility and isothermal reversibility of the heat exchange process are expressed by the values of $\mathrm{Im}[\chi_\alpha]$ and $\mathrm{Re}[\chi_\alpha]$, respectively.[24]

In order to separate the effects of viscosity and thermal conductivity on the stability limit, we calculated the stability limits by setting the value of the Prandtl number σ to 0.71, 0.40, 0.10, and 0. It should be noted that because σ was changed only in the stack, the viscosity outside the stack did not change. The calculated T_H/T_C is shown in Figs. 5(a)–5(c). Since the shape of the stability curves is independent of the values of R, as mentioned in Sec. IV B, only the calculated results with $R=0.15$ m are shown. Since σ for air is nearly 0.71, the curves of the calculated T_H/T_C with $\sigma=0.71$ are almost the same as those shown in Fig. 4(a) by the solid line. Hence, the calculation results with $\sigma=0.71$ are not shown.

In the case investigated by Rott[2] and Yazaki *et al.*,[4] it was claimed that when $\omega\tau_{\alpha,M} \ll 3$, the existence of the stability limit in the tube having two ends can be attributed to the viscosity. However, as shown by the dashed lines in Figs. 4(a) and 5(a)–5(c), T_H/T_C of the straight tube increases with $\omega\tau_{\alpha,M} < 3$, even though σ decreases. This implies that in the present case, the stability limit of the T_H/T_C curve of the straight tube is not necessarily attributable to the viscosity. T_H/T_C of the straight tube takes a minimum value near $\omega\tau_{\alpha,M}=3$ independently of the value of σ. This fact indicates that for the excitation of the gas oscillation in the straight tube, the value of $\omega\tau_\alpha=3$ is important. As shown in Fig. 3, when $\omega\tau_\alpha \sim 3$, $-\mathrm{Im}[\chi_\alpha]$ attains the maximum value and when $\omega\tau \ll 3$, it becomes zero. As mentioned above, $\mathrm{Im}[\chi_\alpha]$ represents the irreversibility of the heat exchange process. Therefore, we can say that the irreversibility of the heat exchange process is indispensable for the excitation of the spontaneous gas oscillation in the straight tube and that when $\omega\tau_{\alpha,M}$ decreases from 3, T_H/T_C of the straight tube increases due to the decrease in the irreversibility.

The solid lines in Figs. 4(c) and 5(a)–5(c) indicate that in the case of the looped tube, the optimum value of $\omega\tau_{\alpha,M}$ for realizing minimum T_H/T_C decreases with a decrease in σ; further, T_H/T_C monotonically decreases at $\sigma=0$. This observation reveals two facts: (1) T_H/T_C increase when $\omega\tau_{\alpha,M} < 3$ in the case of the looped tube, which is shown in Fig. 4(c) by lines, is caused by the viscosity in the stack and (2)

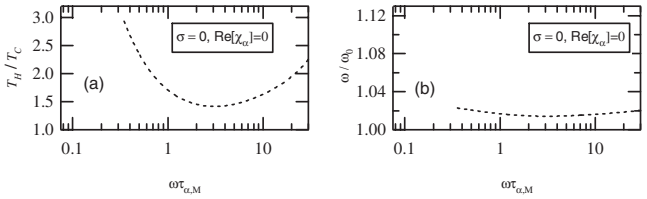

FIG. 6. Stability curves of the straight tube, which is calculated with the assumption that the real part of χ_α, i.e., Re$[\chi_\alpha]$, and σ are both zero.

the isothermal reversibility in the heat exchange process, which is represented by Re$[\chi_\alpha]$, is important for the excitation of the spontaneous gas oscillation in the looped tube. The second fact is considered to contribute to achieving a higher efficiency in the energy conversion occurring in a looped tube as compared with that in a straight tube.

B. Angular frequency ratio ω/ω_0 at the stability limit

The calculated ω/ω_0 with various values of σ is shown in Figs. 5(d)–5(f). When $\sigma=0.71$, ω/ω_0 is not shown due to the above-mentioned reason for not showing T_H/T_C when $\sigma=0.71$. The solid lines in Figs. 4(c), 4(d), and 5(a)–5(g) indicate that the $\omega\tau_{\alpha,M}$ dependence of ω/ω_0 of the looped tube is closely related to T_H/T_C at the stability limit; as T_H/T_C decreases, ω/ω_0 is reduced. This can be considered as proof that ω/ω_0 is determined by the value of the mean sound speed a_m in the tubes because a_m is a function of T_H under a given value of R. In contrast, the $\omega\tau_{\alpha,M}$ dependence of ω/ω_0 of the straight tube cannot be explained by using only a_m. As shown in Figs. 4(a) and 4(b), the T_H/T_C value of the straight tube at $\omega\tau_{\alpha,M}=10$ and 1.5 is 2.1; however, ω/ω_0 at $\omega\tau_{\alpha,M}=10$ and 1.5 is 1.03 and 1.06, respectively. Moreover, ω/ω_0 calculated with various values of σ indicates that the $\omega\tau_{\alpha,M}$ dependence of ω/ω_0 of the straight tube weakly depends on σ, i.e., the value of the viscosity.

The $\omega\tau_{\alpha,M}$ dependence of ω/ω_0 of the straight tube can also be explained by the $\omega\tau_\alpha$ dependence of χ_α. This is because when $\sigma=0$, only χ_α depends on $\omega\tau_\alpha$. In order to split the effects of the imaginary and real parts of χ_α, we set Re$[\chi_\alpha]$ to zero, keeping $\sigma=0$, and calculate the stability limit of the straight tube. The stability limit thus calculated is shown in Fig. 6.

As mentioned above, the T_H/T_C curve of the straight tube for $\omega\tau_{\alpha,M}<3$ exists due to the decrease in $-$Im$[\chi_\alpha]$. Hence, the T_H/T_C curve shown in Fig. 6(a) is U shaped and is very similar to the T_H/T_C curve shown by the dashed line in Fig. 5(c), even though Re$[\chi_\alpha]=0$. However, as observed in Fig. 6(b), the rapid increase in ω/ω_0 with a decrease in $\omega\tau_{\alpha,M}$, which is observed below $\omega\tau_{\alpha,M}<3$ in Fig. 5(f), vanishes; due to this, ω/ω_0 at Re$[\chi_\alpha]=0$ and $\sigma=0$ depends on T_H/T_C. These facts imply that the rapid increase in ω/ω_0 is caused by the $\omega\tau_\alpha$ dependence of Re$[\chi_\alpha]$, while the T_H/T_C curve of the straight tube is determined by the $\omega\tau_\alpha$ dependence of Im$[\chi_\alpha]$.

VI. SUMMARY

The stability limits of the spontaneous gas oscillation thermally induced in the looped and straight tubes were numerically investigated. These numerical results were found to be in qualitative agreement with the measured results. The stability limits were calculated with various values of the Prandtl number of the gas in order to determine the causes of the existence of the stability limit. As a result, it was found that the temperature ratio required for the gas oscillation in the looped tube is determined by the viscosity and isothermal reversibility of the thermal process of heat exchange occurring between the gas and tube wall; however, the temperature ratio required in the straight tube is determined by the irreversibility of the thermal process. On the other hand, the frequency of the gas oscillation occurring in the straight tube depends on the reversibility, whereas the sound speed mainly contributes to the frequency of the gas oscillation occurring in the looped tube.

ACKNOWLEDGMENTS

This research was partially supported by the Ministry of Education, Science, Sports and Culture in Japan under the Grant-in-Aid for Scientific Research (Grant No. 17-10613, 2006) and the Grant-in-Aid for Division of Young Researchers.

[1]N. Rott, "Damped and thermally driven acoustic oscillations," Z. Angew. Math. Phys. **20**, 230–243 (1969).
[2]N. Rott, "Thermally driven acoustic oscillations. Part 2: Stability limit for helium," Z. Angew. Math. Phys. **24**, 54–72 (1973).
[3]N. Rott and G. Zouzoulas, "Thermally driven acoustic oscillations," Z. Angew. Math. Phys. **27**, 197–224 (1976).
[4]T. Yazaki, A. Tominaga, and Y. Narahara, "Experiments on thermally driven acoustic oscillations of gaseous helium," J. Low Temp. Phys. **41**, 45–60 (1980).
[5]W. Arnott, J. Belcher, R. Raspet, and H. Bass, "Stability analysis of a helium-filled thermoacoustic engine," J. Acoust. Soc. Am. **96**, 370–375 (1994).
[6]A. Atchley and F. Kuo, "Stability curves for a thermoacoustic prime mover," J. Acoust. Soc. Am. **95**, 1401–1404 (1994).
[7]N. Sugimoto, "Thermoacoustic oscillations and their stability analysis from a viewpoint of the boundary-layer theory (in Japanese)," Nagare **24**, 381–393 (2005).
[8]N. Sugimoto and M. Yashida, "Marginal condition for the onset of thermoacoustic oscillations of a gas in a tube," Phys. Fluids **19**, 074101 (2007).
[9]T. Yazaki, S. Takashima, and F. Mizutani, "Complex quasiperiodic and chaotic states oeserved in thermally induced oscillations of gas columns," Phys. Rev. Lett. **58**, 1108–1111 (1987).
[10]S. Backhaus, E. Tward, and M. Petach, "Traveling-wave thermoacoustic electric generator," Appl. Phys. Lett. **85**, 1085–1087 (2004).
[11]E. Luo, W. Dai, Y. Zhang, and H. Ling, "Thermoacoustically driven refrigerator with double thermoacoustic-stirling cycles," Appl. Phys. Lett. **88**, 074102 (2007).
[12]T. Yazaki, T. Biwa, and A. Tominaga, "A pistonless stirling cooler," Appl. Phys. Lett. **80**, 157–159 (2002).
[13]P. Ceperley, "A piston-less stirling engine," J. Acoust. Soc. Am. **65**, 1508–1513 (1979).
[14]S. Backhaus and G. W. Swift, "A thermoacoustic stirling engine," Nature (London) **399**, 335–338 (1999).
[15]T. Yazaki, A. Iwata, T. Mackawa, and A. Tominaga, "Traveling wave thermoacoustic engine in a looped tube," Phys. Rev. Lett. **81**, 3128–3131 (1998).
[16]H. Tanaka, "Investigation of thermoacoustic phenomena," MS thesis, The University of Tokyo, Tokyo, 2002.
[17]G. Penelet, S. Job, V. Gusev, P. Lotton, and M. Bruneaua, "Dependence of sound amplification on temperature distribution in annular thermoacoustic engines," Acust. Acta Acust. **91**, 567–577 (2005).
[18]G. W. Swift, *Thermoacoustics: A Unifying Perspective for Some Engines and Refrigerators* (Acoustical Society of America, Pennsylvania, 2002).
[19]T. Yazaki, Y. Tashiro, and T. Biwa, "Measurements of sound propagation

in narrow tubes," Proc. R. Soc. London, Ser. A **463**, 2855–2862 (2007).
[20]R. S. Wakeland and R. M. Keolian, "Measurements of the resistance of parallel-plate heat exchangers to oscillating flow at high amplitudes," J. Acoust. Soc. Am. **115**, 2071–2074 (2004).
[21]*JASM Data Book:Thermophysical Properties of Fluids* (the Japan Society of Mechanical Engineers, Tokyo, 1983).
[22]The hydraulic diameter d_h is defined as $d_h=4V_{\mathrm{gas}}/A_{\mathrm{gas\text{-}solid}}$, where V_{gas} is the gas volume and $A_{\mathrm{gas\text{-}solid}}$ is the gas-solid contact surface area.
[23]W. Arnott, H. Bass, and R. Raspet, "General formulation of thermoacoustics for stacks having arbitrarily shaped poro cross sections," J. Acoust. Soc. Am. **90**, 3228–3237 (1991).
[24]A. Tominaga, "Therммodynamic aspect of thermoacoustic phenomena," Cryogenics **35**, 727–440 (1995).